J. Fluid Mech. (2010), *vol.* 655, *pp.* 504–514.
doi:10.1017/S0022112010001229

Convective instability in steady stenotic flow: optimal transient growth and experimental observation

M. D. GRIFFITH[1]†, M. C. THOMPSON[1], T. LEWEKE[2] AND K. HOURIGAN[1]

[1]Fluids Laboratory for Aeronautical and Industrial Research (FLAIR), Department of Mechanical and Aerospace Engineering and Division of Biological Engineering, Monash University, Melbourne, Victoria 3800, Australia

[2]Institut de Recherche sur les Phénomènes Hors Equilibre (IRPHE), CNRS/Universités Aix-Marseille, 49 rue Frédéric Joliot-Curie, BP 146, F-13384 Marseille Cedex 13, France

(Received 26 November 2009; revised 7 March 2010; accepted 8 March 2010; first published online 16 April 2010)

An optimal transient growth analysis is compared with experimental observation for the steady flow through an abrupt, axisymmetric stenosis of varying stenosis degree. Across the stenosis range, a localized sinuous convective shear-layer instability type is predicted to dominate. A comparison of the shape and development of the optimal modes is made with experimental dye visualizations. The presence of the same sinuous-type disturbance immediately upstream of the highly chaotic region observed in the experimental flow is consistent with the optimal growth predictions. This, together with the fact that the flow is unstable globally only at much higher Reynolds numbers, suggests bypass transition.

1. Introduction

The flow through a straight pipe with a contraction serves as an idealized model of the arterial flow through an atherosclerotic stenosis; although somewhat removed from the physiological reality of an arterial stenosis, the understanding of the flow in the simplified model is of importance to studying further the flows in more complicated models.

Experimental investigation (Khalifa & Giddens 1981; Ahmed & Giddens 1984; Ohja *et al.* 1989; Griffith *et al.* 2008, 2009) has determined regions of transitional flow in the post-stenotic region, for Reynolds numbers and blockage sizes common to physiological arterial blockages. Via direct numerical simulation, similar behaviour has been observed computationally (Mallinger & Drikakis 2002; Varghese, Frankel & Fischer 2007). Linear Floquet stability and optimal transient growth analysis have been used to identify instability modes on the axisymmetric base flow (Sherwin & Blackburn 2005; Blackburn, Sherwin & Barkley 2008); in general, it has been established that shear-layer convective instabilities play an important role in the transition of such flows, appearing at Reynolds numbers much lower than those predicted by a linear asymptotic stability analysis.

The intent of this study is to extend previous work (Griffith *et al.* 2008), where the steady flow through a pipe with an abrupt, axisymmetric stenosis of varying

† Email address for correspondence: martin.griffith@eng.monash.edu.au

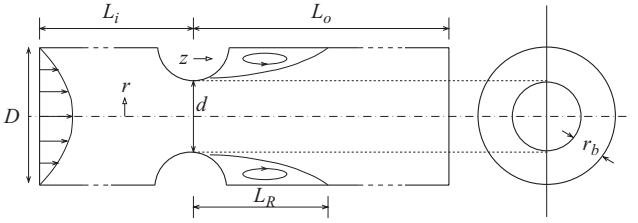

FIGURE 1. Schematic of the geometry under investigation.

blockage size was investigated experimentally and numerically. In Griffith *et al.* (2008), it was shown experimentally that the steady flow in a straight pipe with an axisymmetric stenosis became unstable at Reynolds numbers of roughly one-half of those predicted by the global stability analysis. The observed form of the instability was an axisymmetric roll-up of the shear-layer immediately downstream of the blockage; small Kelvin–Helmholtz-type vortices were observed to advect downstream and grow before reaching an unsteady region of flow farther downstream. The analysis focused on the near-wake region, presenting results and comparisons between the roll-up of the shear layer and the effects of forced-frequency perturbations on axisymmetric simulations. For the steady flow through a similar geometry, Blackburn *et al.* (2008) identified optimal perturbations to the steady axisymmetric base flow for the maximal energy growth. For steady flow, the perturbation to the field was found to be distinctly sinuous.

In the present investigation, an optimal transient energy growth analysis is performed on the stenosis configuration, over a range of blockage degrees, and a comparison is made with the results of experimental observations for the same geometry. Such a comparison was not achieved in Griffith *et al.* (2008), where the global linear stability analysis used was not able to capture the convective instabilities that appear to be responsible for the downstream turbulent transition.

Section 2 presents a precis of the problem investigated, followed by a description of the techniques used in the study in § 3. Results and discussion are given in §§ 4 and 5, respectively.

2. Problem definition

The geometry under investigation is identical to the one used in Griffith *et al.* (2008) and is reproduced in figure 1. It consists of a long straight tube with an axisymmetric blockage described by a single parameter, the stenosis degree, representing the blocked to unblocked area ratio, defined as $b = 1 - (d/D)^2$, where D is the diameter of the tube and d is the diameter at the centre of the blockage. The fluid is assumed to be Newtonian. The Reynolds number is defined as $Re = \overline{U}D/\nu$, where $\overline{U}$ is the sectionally averaged fluid velocity, D is the tube diameter, and ν is the kinematic viscosity. The coordinate system is such that the origin ($(r, z) = (0, 0)$) is located on the centreline of the tube at the axial mid-point of the stenosis. In this paper, we examine Reynolds numbers between 100 and 1000, with stenosis degrees of $b = 0.50$, 0.60, 0.75 and 0.90. Lengths and times are non-dimensionalized by D and $D/\overline{U}$, respectively.

The steady base flow downstream of any size of blockage consists of a jet emanating from the constriction. The adverse pressure gradient over the stenosis causes separation, with a long, thin recirculation zone forming immediately after the

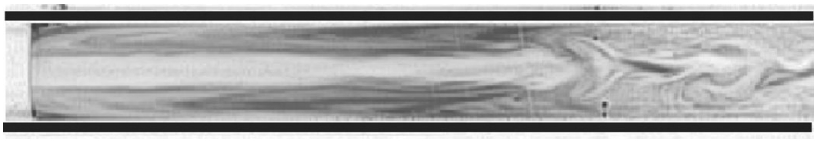

FIGURE 2. Dye visualization of the unsteady flow for $b = 0.90$ and $Re = 190$. The visible region of the flow begins immediately downstream the stenosis at $z = r_b$.

stenosis. A linear stability analysis shows that the flow becomes linearly unstable at $Re = 770$ for $b = 0.75$ and at $Re = 395$ for $b = 0.90$. For both these cases, the leading instability mode is of wavenumber $k = 1$, consisting of a deflection of the jet from the centreline of the tube. For smaller stenosis degrees, $b = 0.50$ and $b = 0.60$, the leading instability mode changes, with a $k = 2$ mode dominating. The mode has a plane of symmetry, consisting of a pinching of the jet (Griffith *et al.* 2008).

Experimentally, the flow is far less stable. Figure 2 shows a dye visualization for $b = 0.90$ and $Re = 190$. The instability manifests as a convective Kelvin–Helmholtz-type instability, beginning in the shear layer downstream of the stenosis. The Kelvin–Helmholtz-type vortices are small, yet fairly well-defined; after travelling downstream and growing, the vortices terminate in a large area of disturbance. This study examines in a closer detail the region immediately before this highly chaotic region.

For the present experimental configuration, the flow becomes unstable for $b = 0.50$ at $Re_c \approx 900$, for $b = 0.75$ at $Re_c \approx 400$ and for $b = 0.50$ at $Re_c \approx 150$. We focus on these Reynolds numbers in our optimal perturbation analysis.

3. Method

3.1. *Numerical simulations*

Two-dimensional axisymmetric flow simulations are obtained from a numerical solution of the time-dependent Navier–Stokes equations using the spectral-element method (see e.g. Thompson, Hourigan & Sheridan 1996 or Thompson *et al.* 2006). On the stenosis surface and the cylinder walls, no-slip conditions are imposed. At the inlet boundary, an equilibrium Poiseuille profile is prescribed. At the outflow boundary far downstream, the standard zero normal velocity gradient condition is imposed. The simulations are initialized with the fluid at rest and run until the flow has achieved a converged and steady state. Further information on the method, meshing and resolution testing can be found in Griffith *et al.* (2008).

From the two-dimensional axisymmetric simulations and computed optimal perturbation modes (as discussed below), a three-dimensional optimally perturbed velocity field can be constructed. This can be integrated forward in time to determine the linear and nonlinear flow behaviour as the perturbation, which is initially localized near the throat, is convected downstream. The same spatial discretization as the two-dimensional simulations is employed in the three-dimensional solver, along with a Fourier decomposition in the azimuthal direction. In these simulations, Lagrangian particle tracking is employed. This involves the continuous feeding of particles into the flow at carefully chosen locations; the instantaneous particle positions can then be used to create images that are effectively simulated dye visualizations. By tracking the development of selected numerical perturbations on the flow field, the results can be directly compared with images from the dye-visualization experimental technique described in § 3.3.

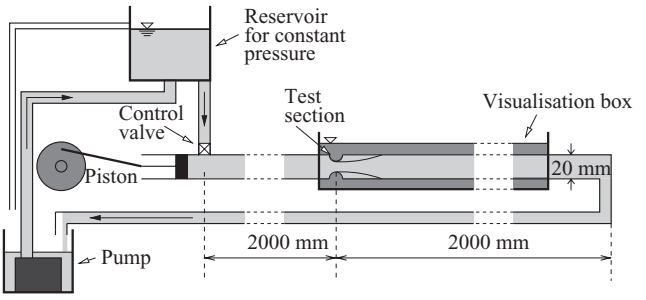

FIGURE 3. Schematic of the experimental rig; the inlet and outlet lengths have been truncated.

3.2. *Optimal transient energy growth analysis*

The method used on the numerically simulated flows for the optimal transient growth analysis is presented in detail by Schmid & Henningson (2001) and Barkley, Blackburn & Sherwin (2008). For a given time interval τ the method determines the linear perturbation velocity field $\boldsymbol{u}'(r, \theta, z)$ of the azimuthal wavenumber k, which produces the greatest growth G in the L_2 energy norm at $t = \tau$ on the steady axisymmetric base flow $\overline{\boldsymbol{u}}(r, z)$. Stated more simply, the aim is to find the shape of the perturbation that leads to a maximal energy amplification, G, over some specified time, τ. The global maximum of G for a given wavenumber is denoted by G_{max}, with its corresponding τ denoted by τ_{max}. Asymptotically, the modes are stable. However, the transient disturbance the modes cause in the flow can be of sufficient magnitude to cause the flow to become nonlinear. This can lead to bypass transition at Reynolds numbers considerably lower than those predicted by the linear absolute stability analysis. This is particularly the case for flows of long, thin shear layers – such as for the present geometry – where convective instabilities are able to grow for a relatively long time as they advect along separating shear layers.

3.3. *Experimental method*

A description of the experimental apparatus in more depth than the short summary included here can be found in Griffith *et al.* (2008). A schematic of the rig design is shown in figure 3. It consists of a transparent perspex tube of 20 mm diameter, with inlet and outlet lengths of 2000 mm, or $100D$. This ensures a fully developed Poiseuille flow at the test section, free of any end effects. The three removable test sections constructed correspond to stenosis degrees of $b = 0.50$, 0.75 and 0.90. The test section and outlet length are contained in a rectangular water-filled viewing box. A pump supplies an elevated water reservoir, thereby keeping the pressure in the system constant. The Reynolds number is varied via a control valve located before the entry into the inlet tube.

The flow is analysed primarily using coloured dye visualization. Fluoroscein dye is injected into the flow immediately downstream of the stenosis and a vertical plane of the flow is illuminated by a laser light sheet. The technique is effective in delineating the recirculation zone and shear layer of the separated flow. The dye trapped in a steady recirculation zone contrasts with the dye-free fluid arriving from upstream. The dye serves as a useful indicator for any unsteadiness present in the flow.

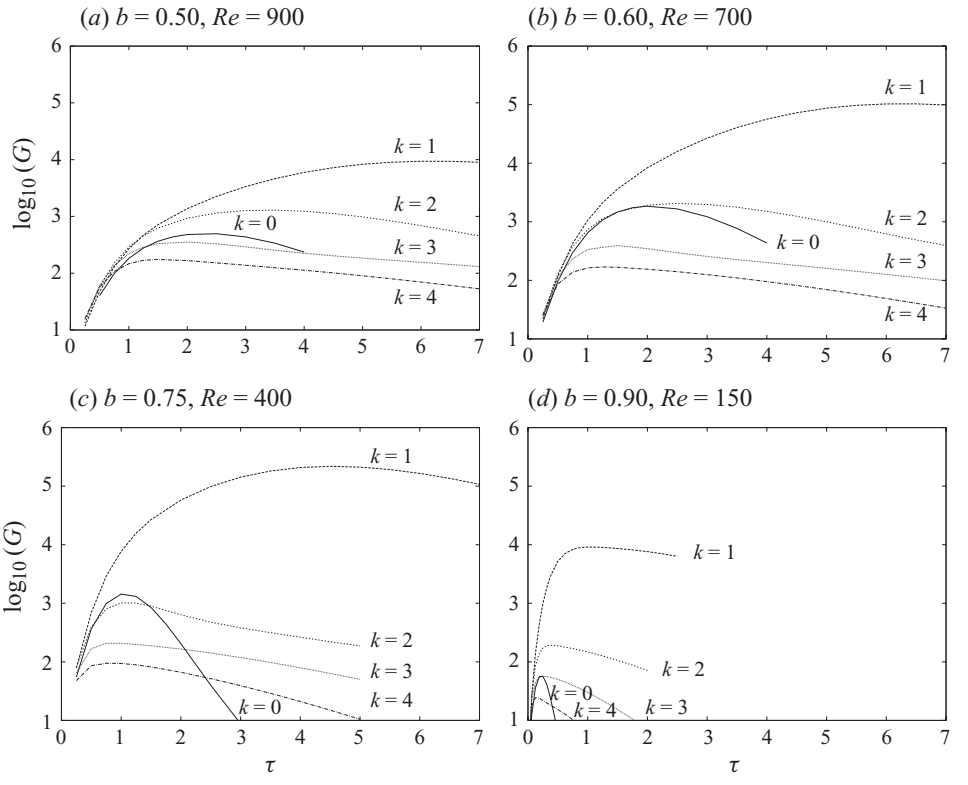

FIGURE 4. Log plots of transient energy growth, G, for given τ, at different blockage ratios for azimuthal wavenumbers $k = 0$ to $k = 4$.

4. Results

4.1. *Transient energy growth*

Figure 4 shows $\log_{10}$ of the transient energy growth, G, for optimal disturbances as functions of τ for the steady base flow for four different stenosis degrees: $b = 0.50$, 0.60, 0.75 and 0.90. The Reynolds number chosen for the analysis in each stenosis degree case corresponds to the lowest Reynolds numbers at which the flow was observed to be unstable experimentally (Griffith *et al.* 2008). For the $b = 0.60$ case, which was not tested experimentally, the Reynolds number used has been interpolated to $Re = 700$, from the other cases tested. In each case, energy growth for azimuthal wavenumbers $k = 0$ to $k = 4$ is plotted. For all cases tested, the mode of $k = 1$ produces the greatest energy.

Figure 5 plots the azimuthal vorticity fields of the optimal initial perturbations for the four cases tested. In each, the perturbation maximum is located in the vicinity of the separation point of the blockage. Located here, the perturbation travels along the separating shear layer as long as possible, hence providing the optimal growth. The basic nature of the disturbance does not vary with the stenosis degree.

Note the choice of Reynolds numbers and the resulting energy growths. The global maxima of energy vary significantly across the stenosis degree range; for $b = 0.50$, it occurs for $\tau_{max} = 6.21$ for an energy maximum $G_{max} = 9.42 \times 10^3$; for $b = 0.75$, the optimum occurs at $\tau_{max} = 4.54$ for an energy maximum of 2.18×10^5. The Reynolds numbers were chosen according to where the flow is seen to be

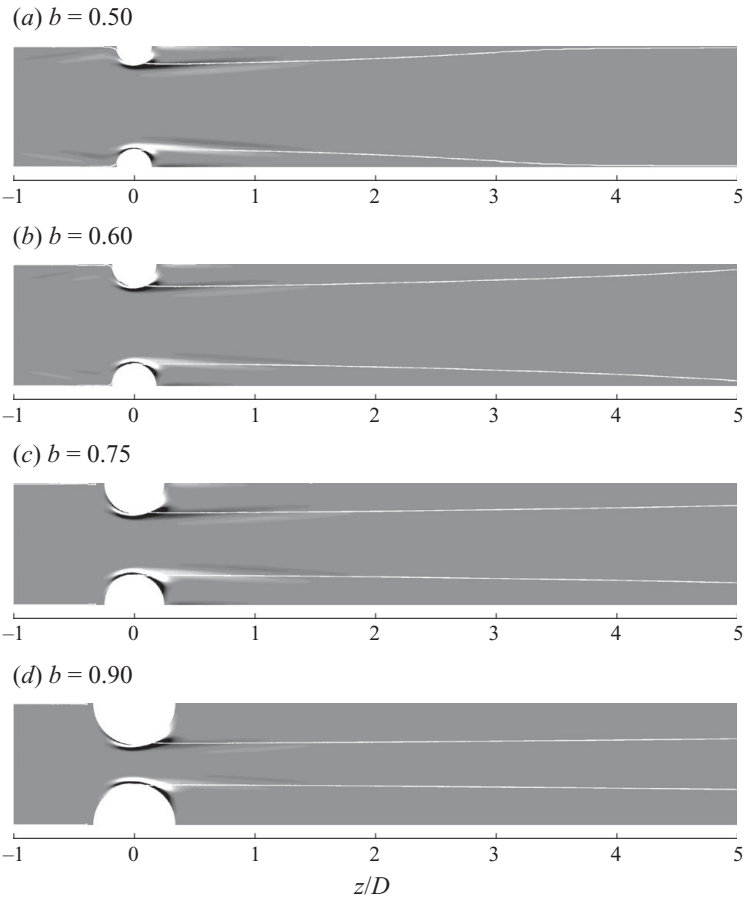

FIGURE 5. Plots of azimuthal vorticity of the optimal initial perturbation (all $k = 1$) for the four different cases tested, at stenosis degrees $b = 0.50$, 0.60, 0.75 and 0.90, for the leading τ. The separating streamline of the stable axisymmetric base flow is overlaid in each case.

unstable in the experimental flow (Griffith *et al.* 2008). By intentionally introducing more noise or driven-frequency perturbations into the experimental flow, it was also observed that the instability in the experiments was at least partially dependent on the background noise. It is reasonable to expect that changing the blockage test section in the experiment could change the amount of background noise in the experiment. Furthermore, in Blackburn *et al.* (2008), it was shown that the global energy maxima obtained through the transient energy growth analysis increases exponentially with the Reynolds number; therefore, any discrepancy in the critical Reynolds number obtained experimentally may be reflected in the varying global energy maxima seen in figure 4. An interesting point is that for each blockage ratio, at the experimentally observed transition Reynolds number the maximal energy amplification factor is approximately 10^4–10^5. This appears to be reasonably consistent with a background experimental noise level of around 1 %; i.e. a growth of velocity perturbations by a factor $\sqrt{10^4} = 100$ will mean that the perturbation level grows to the same order as the velocity field, at which point the flow should become nonlinear, resulting in transition.

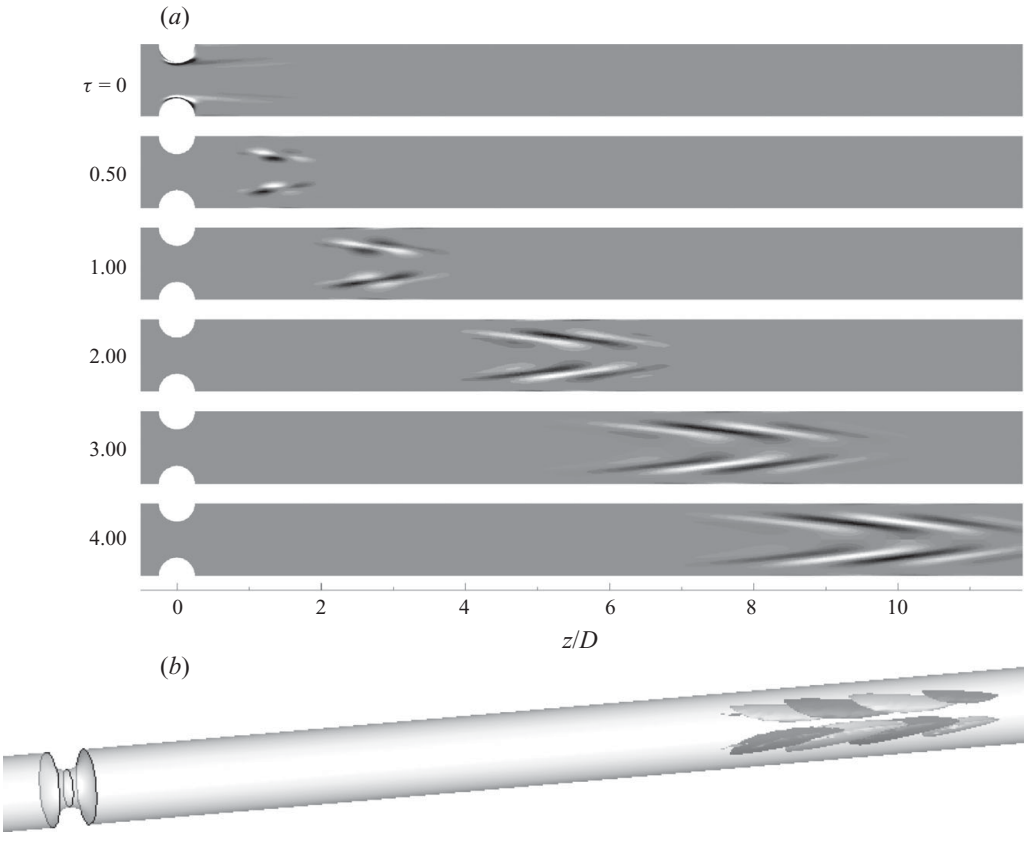

FIGURE 6. (*a*) Series of images of the azimuthal vorticity of the optimal disturbance for $b = 0.75$, $Re = 400$, $k = 1$, showing the development of the perturbation. Vorticity contours have been progressively enlarged in each image to show the features of the flow. (*b*) Three-dimensional view of the perturbation at maximal energy showing two opposite sign isosurfaces of axial vorticity. Flow is from left to right.

The results of figure 4(*c*) compare well with the analysis carried out by Blackburn *et al.* (2008). In that study, a global maximum of energy growth was found for $\tau = 4.40$ and $k = 1$ of $G_{max} = 8.94 \times 10^4$, about 40 % of the value found here. The difference in energy growth can be accounted for if we consider the differences in the two problem configurations. The analysis of Blackburn *et al.* (2008) used the same Reynolds number and stenosis degree, but a stenosis geometry of a co-sinusoidal shape with an axial length twice that of the present geometry. The shorter, more abrupt blockage of the present study results in a greater acceleration of the fluid through the constriction, which in turn produces thinner shear layers. The optimal initial perturbations are all located in the thinnest part of the separating shear layer; the greater maximum energy found reflects the greater propensity for instability in thinner shear layers.

Figure 6(*a*) presents the development of the $k = 1$ optimal perturbation field for $b = 0.75$ and $Re = 400$, using a series of images showing the azimuthal vorticity of the disturbance from the initial state to the state of maximal energy. The disturbance consists of a sinuous wave packet; the maximum rate of growth occurs at the beginning of the series (figure 4*c*), when the perturbation passes through

the thinnest part of the shear layer, immediately downstream of the stenosis. As the shear layer expands and the recirculation zone tails away, the growth slows and the axial wavelength of the disturbance increases. The sinuous nature of the perturbation can be seen in figure 6(*b*), which shows another view of the disturbance at the point of maximal energy, $\tau = \tau_{max}$. After this point, the energy in the disturbance passes into a less unstable region and decays.

4.2. *Experimental comparison*

In the experimental observations of Griffith *et al.* (2008), the observable disturbances were the focus. The small well-defined waves evident in the shear layers immediately downstream of the blockage provided quantitative measures of the unsteadiness. This is in contrast to the region of strong unsteadiness further downstream, from which clear quantitative observations using the dye-visualization technique were more difficult to obtain. However, in light of the results presented in the previous section – in particular, the large growth in the disturbance further downstream – it is in this region of the flow that meaningful comparison between our numerics and the experimental results may be possible.

The experimental dye visualizations, some of which are presented by Griffith *et al.* (2008), have been re-analysed with reference to the numerical results of the previous section. A comparison of the perturbation field at the axial location of the maximum vorticity at $\tau = \tau_{max}$ with the corresponding experimental dye visualization is not particularly useful, because by that stage the perturbation has grown so much that the interaction with the base flow is nonlinear. At these axial locations (e.g. $z/D \approx 12$ for $b = 0.75$ and $Re = 400$), the experimental flow is highly unsteady; the dye is mixed and does not show any meaningful structure. For this reason, comparisons of the nearer-wake region are the focus of this study. In Griffith *et al.* (2008), shear-layer waves that developed immediately downstream of the stenosis were reported. In that analysis, those waves were observed to be axisymmetric, that is, the waves observed on the shear layer in the top half of the laser sheet matched those observed on the shear layer in the bottom half. However, as the waves grew and advected towards the unsteady region downstream, there was no obvious continuous transition between the upstream axisymmetric near-wake region and the downstream highly unsteady region.

From the results of the optimal perturbation analysis indicating maximal growth for sinuous (i.e. $k = 1$) disturbances, a re-examination of the experimental visualizations was conducted with a focus on detecting such disturbances. In the majority of cases, across the three stenosis degrees tested experimentally, no sinuous disturbance was detectable. For the $b = 0.50$ case, no cases were found exhibiting the sinuous behaviour. However, for the $b = 0.75$ and $b = 0.90$ cases, several cases were found exhibiting the sinuous behaviour. Comparison was made in the near-wake region with the developing perturbation fields at $\tau < \tau_{max}$, that is, at axial locations upstream of where the maximal energy occurs in the numerics.

Figure 7 shows two such cases, where comparison is possible with the optimal transient energy growth analysis of § 4.1. Figure 7(*a*) shows a dye visualization of the flow for $b = 0.75$ and $Re = 457$. For this case, the transient growth analysis finds a maximal energy growth for the $k = 1$ mode, for $\tau_{max} = 5.15$. Directly beneath this image is a simulated dye-visualization image obtained from Lagrangian particle tracking on the evolving flow, initially consisting of the optimal perturbation mode at a low amplitude, plus the three-dimensional axisymmetric base flow. To produce this image, the particles are released at a constant rate on the surface of the stenosis; in this

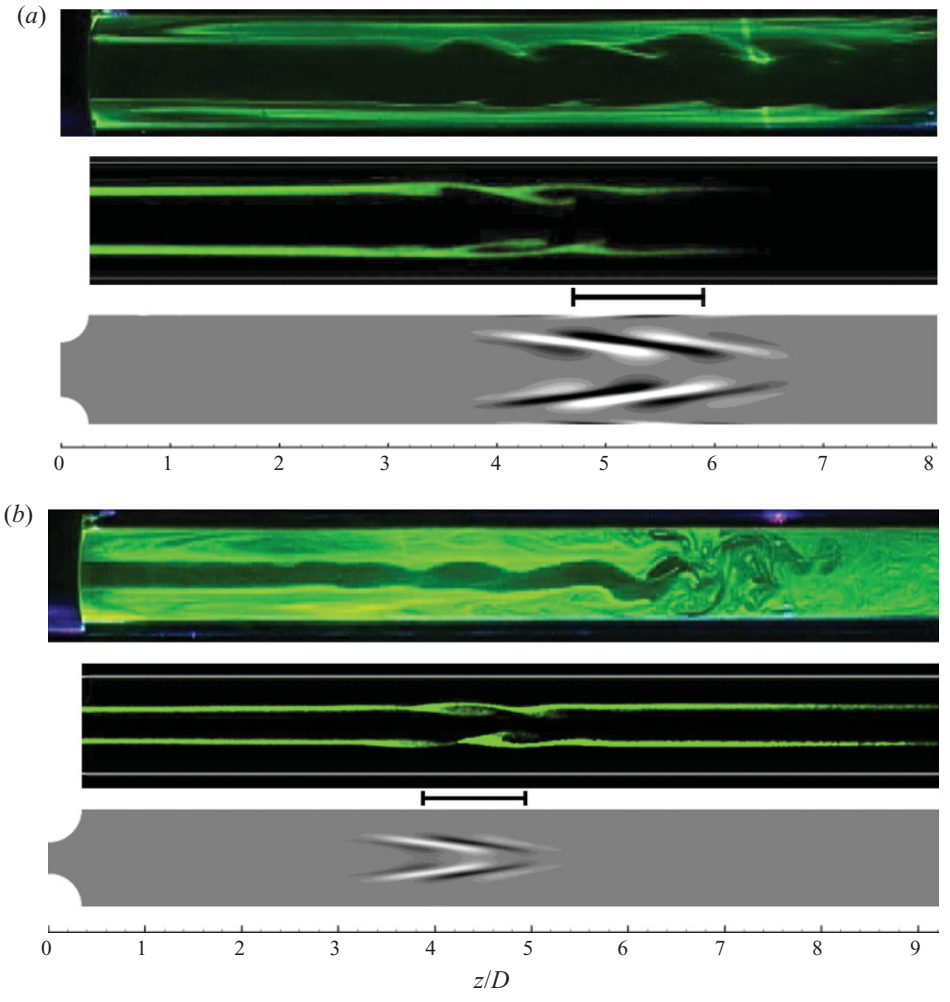

FIGURE 7. (*a*) For stenosis degree $b = 0.75$, Reynolds number $Re = 457$; at the top is plotted an experimental dye visualization of the flow; in the middle, Lagrangian particle traces (shown in a single meridional plane) from a perturbed three-dimensional simulation of the same flow. Below that, for reference, the azimuthal vorticity of the developing perturbation is shown at $\tau = 1.9$. Similarly, in (*b*), for $b = 0.90$ and $Re = 215$, the maximal energy is reached at $\tau_{max} = 1.38$, but for comparison between the experimental dye visualization and the perturbation azimuthal vorticity, the field is plotted at $\tau = 0.6$. The black lines indicate where the comparison in the axial wavelength of the disturbance may be made.

way, the particles aggregate along the separating shear layer. This is in contrast to the experiment, where the dye is heavily mixed in the recirculation zone. However, both techniques achieve the same end, in which the dye/particles highlight disturbances growing along the shear layer. For reference, the third subfigure shows contours of azimuthal vorticity of the perturbation field for optimal growth ($k = 1$, $\tau_{max} = 5.15$) at $\tau = 1.90$. Similar sinuous-type structures can be observed in the experimental and numerical 'dye' visualizations. The axial wavelength of this disturbance is of a similar magnitude to that of the growing perturbation field. A similar comparison is made in figure 7(*b*), this time for $b = 0.90$ and $Re = 215$ ($\tau_{max} = 1.38$); the perturbation field is

plotted at $\tau = 0.60$. Again, the same axial wavelength is observed in the perturbation field, as in the disturbance of the experimental and numerical 'dye' visualizations.

The comparisons shown in figure 7 are good, with both numerical and experimental results exhibiting the same sinuous-type behaviour; however, as pointed out previously the sinuous motion is clearly observable experimentally only in limited cases and even then only intermittently. There are several possible explanations for this. The optimal perturbations plotted in figures 5 and 6 possess a plane of symmetry. While the sinuous perturbation of our numerics always acts in line with the page, in the experiment, the disturbance may act in any direction. While there is evidence that buoyancy can affect some form of instability (Griffith *et al.* 2009), we are unaware of the extent to which the sinuous disturbance may act out of the plane of the vertical laser light sheet. Also note that figure 4 shows that the 'initial' growth rates of modes with different azimuthal dependence are similar. Thus, the near wake will be dominated by the combination of modes with the highest initial amplitude. This is a function of the spatial and temporal distribution of experimental noise or other perturbations to the flow/rig. Thus, it is not surprising that the very near wake does not necessarily show dominance of the $k = 1$ mode. However, further downstream, figure 4 shows that the $k = 1$ mode should dominate provided the growth of other modes has not already caused the flow to become nonlinear. Finally, figure 4 shows that there is a much greater difference in the growth of the $k = 1$ mode compared with other modes for larger τ, for the two higher blockage ratios. This indicates that it may be easier to find experimental evidence of the $k = 1$ mode for $b = 0.75$ and $b = 0.90$ than for $b = 0.50$, and indeed this is the case.

As well as possibly accounting for the seemingly axisymmetric disturbances observed experimentally by Griffith *et al.* (2008), these factors indicate the operation of a bypass transition. These factors include the large growths found by the optimal transient growth analysis and the presence of the same (asymptotically stable) modes in the regions of sustained unsteadiness in the experimental flow.

5. Conclusions

An optimal transient energy growth analysis of the steady base flow through an axisymmetric stenosis has been presented, for a number of different stenosis degrees, at approximate Reynolds numbers where unsteadiness is expected experimentally. The modes achieving the greatest energy growth consist of optimal initial disturbances located in the separation points on the stenoses, which then advect downstream, growing into longer wavelength sinuous disturbances. Limited though strong comparisons were made with experimental observations, indicating the action of bypass transition.

The authors gratefully acknowledge financial support from the Australian Research Council (ARC Discovery Project grant DP0555897 and ARC Linkage International grant LX0668992), the Australian Academy of Science and the Embassy of France in Australia.

REFERENCES

Ahmed, S. A. & Giddens, D. P. 1984 Pulsatile poststenotic flow studies with laser Doppler anemometry. *J. Biomech.* **17**, 695–705.

Barkley, D., Blackburn, H. M. & Sherwin, S. J. 2008 Direct optimal growth analysis for timesteppers. *Intl J. Numer. Meth. Fluids* **57**, 1435–1458.

Blackburn, H. M., Sherwin, S. J. & Barkley, D. 2008 Convective instability and transient growth in steady and pulsatile stenotic flow. *J. Fluid Mech.* **607**, 267–277.

Griffith, M. D., Leweke, T., Thompson, M. C. & Hourigan, K. 2008 Steady inlet flow in stenotic geometries: convective and absolute instabilities. *J. Fluid Mech.* **616**, 111–133.

Griffith, M. D., Leweke, T., Thompson, M. C. & Hourigan, K. 2009 Pulsatile flow in stenotic geometries: flow behaviour and stability. *J. Fluid Mech.* **622**, 291–320.

Khalifa, A. M. A. & Giddens, D. P. 1981 Characterization and evolution of poststenotic disturbances. *J. Biomech.* **14**, 279–296.

Mallinger, F. & Drikakis, D. 2002 Instability in three-dimensional, unsteady, stenotic flows. *Intl J. Heat Fluid Flow* **23**, 657–663.

Ohja, M., Cobbold, R. S. C., Johnston, K. W. & Hummel, R. L. 1989 Pulsatile flow through constricted tubes: an experimental investigation using photochromic tracer methods. *J. Fluid Mech.* **203**, 173–197.

Schmid, P. J. & Henningson, D. S. 2001 *Stability and Transition in Shear Flows*. Springer.

Sherwin, S. J. & Blackburn, H. M. 2005 Three-dimensional instabilities of steady and pulsatile axisymmetric stenotic flows. *J. Fluid Mech.* **533**, 297–327.

Thompson, M. C., Hourigan, K., Cheung, A. & Leweke, T. 2006 Hydrodynamics of a particle impact on a wall. *Appl. Math. Mod.* **30** (11), 1356–1369.

Thompson, M. C., Hourigan, K. & Sheridan, J. 1996 Three-dimensional instabilities in the wake of a circular cylinder. *Exp. Therm. Fluid Sci.* **12**, 190–196.

Varghese, S. S., Frankel, S. H. & Fischer, P. F. 2007 Direct numerical simulation of stenotic flows. Part 1. Steady flow. *J. Fluid Mech.* **582**, 253–280.